Functional truncations for the solution of the nonperturbative RG equations

IOP Publishing Journal of Physics A: Mathematical and Theoretical
J. Phys. A: Math. Theor. **55** (2022) 465002 (24pp) https://doi.org/10.1088/1751-8121/ac9f8c

Functional truncations for the solution of the nonperturbative RG equations

J Kaupužs[1,2,3,*] **and R V N Melnik**[3,4]

[1] Laboratory of Semiconductor Physics, Institute of Technical Physics, Faculty of Materials Science and Applied Chemistry, Riga Technical University, P. Valdena 3/7, Riga LV-1048, Latvia
[2] Institute of Science and Innovative Technologies, University of Liepaja, 14 Liela Street, Liepaja LV–3401, Latvia
[3] The MS2 Discovery Interdisciplinary Research Institute, Wilfrid Laurier University, Waterloo N2L 3C5, Ontario, Canada
[4] BCAM—Basque Center for Applied Mathematics, E48009 Bilbao, Spain

E-mail: kaupuzs@latnet.lv

Received 16 March 2022; revised 27 October 2022
Accepted for publication 2 November 2022
Published 22 November 2022

Abstract

We consider the Wetterich exact renormalization group (RG) equation. Approximate closed equations are obtained from it, applying certain truncation schemes for the effective average action. These equations are solved either purely numerically or by certain extra truncations for the potential and related quantities, called the functional truncations. Traditionally, the functional truncations consist of truncated expansions in powers of $\tilde{\rho}-\tilde{\rho}_0$, where $\tilde{\rho}\propto\phi^2$, ϕ is the averaged order parameter, and $\tilde{\rho}_0$ corresponds to the minimum of the dimensionless potential $u_k(\tilde{\rho})$, depending on the infrared cut-off scale k. We propose a new approach of functional truncations, using the expansion $u_k(\tilde{\rho})-u_k(0)=(1-s)^{-\mu}\left(u_{1,k}s+u_{2,k}s^2+\cdots\right)$, where $s=\tilde{\rho}/(\tilde{\rho}_0+\tilde{\rho})$, $\tilde{\rho}_0$ is an optimization parameter and μ is the exponent, describing the $\tilde{\rho}\to\infty$ asymptotic. The newly developed method provides accurate estimates of the critical exponents η, ν and also ω. In the case of the local potential approximation (LPA), the discrepancy with the purely numerical solution is 0.000 15 for ν and 0.0012 for ω at the s^{13} order of truncation. We show that this method is advantageous for estimations beyond the LPA, especially, for the critical exponent ω. In particular, we have obtained $\eta=0.0454(1)$, $\nu=0.6292(2)$, and $\omega=0.8606(30)$ for the equation originally derived in 2020 *J. Phys. A: Math. Theor.* **53** 415002 within a new truncation scheme for the effective action.

* Author to whom any correspondence should be addressed.

The approach can also be used for the solution of other nonperturbative RG models that have a broad range of applications.

Keywords: functional renormalization, Wetterich equation, functional truncations, exact renormalization group equations, non-perturbative approaches, quantum and statistical field theories, strongly interacting systems

1. Introduction

The renormalization group (RG) method is one of the most widely used approaches in the analysis of critical phenomena [1–5]. Here we will consider the non-perturbative RG approach [6–9], focusing on the Wetterich equation and its approximation schemes, developing further the research initiated in [10].

The functional-RG approach, which is at the heart of such models as the Wetterich and the Polchinski equations, provides an appropriate framework for the analysis of a range of central problems in such areas as, e.g. quantum gravity, Yang–Mills theories and non-relativistic quantum systems, as well as statistical physics—see, e.g. [11] for a recent review. The non-perturbative RG equations have been already applied to many particular systems, including the Ginzburg–Landau model [10–19], quantum systems and quantum gravity [20–31] and the tensorial group field theory [32].

While the Wetterich equation itself is exact, it cannot be solved exactly. Approximate closed equations are obtained from it, applying certain truncation schemes for the effective action. The local potential approximation (LPA) is a widely known lowest-order approximation, which is traditionally improved step by step by the derivative expansion (DE) [9, 14, 15]. As alternative truncation schemes, the vertex expansion [15], the BMW scheme [18] and the recent scheme proposed in [10] can be mentioned. In distinction to the DE, which relies on the small momentum (wave-vector magnitude) approximation, the latter two schemes preserve the full momentum dependence. In the BMW scheme, however, it is only taken into account up to a certain order, assuming a simplified momentum dependence for the highest-order vertices considered.

We have developed a new scheme of semi-analytic approximations or functional truncations for the solution of the truncated non-perturbative RG flow equations. By 'functional truncations' we mean truncations for the potential and related quantities. These truncations are applied atop of those for the effective average action. Our new scheme of the functional truncations is proposed as an alternative to the already existing ones [9, 14, 15], as well as to the purely numerical solutions [11, 18, 19] of the RG flow equations, obtained at a given order of DE, BMW or any other scheme, which contains functions of ϕ^2 with ϕ being the mean order parameter of the effective average action.

The traditional functional truncation scheme relies on the expansions in powers of $\tilde{\rho} - \tilde{\rho}_0$, where $\tilde{\rho} \propto \phi^2$ and $\tilde{\rho}_0$ corresponds to the potential minimum (see section 3 for further details). The critical exponents η and ν, extracted by this method from the LPA and DE equations, have been reported, e.g. in [14–16]. To the best of our knowledge, the results of these functional truncations have been limited to the LPA case [16] for the correction-to-scaling exponent ω. Our new method allows to obtain more accurate values of ω, going beyond the LPA. Such values have been obtained in [11, 18, 19] from purely numerical solutions of the resulting approximate closed RG flow equations at a given order. However, when dealing with applied problems, the purely numerical approach faces several challenges such as the numerical instability and the need of a relatively large computational effort. In particular, numerical

instability was an obstacle for the extension of the results of the BMW truncation scheme beyond the first approximation [18]—see the discussion at the end of appendix B in [18]. The new semi-analytic approximations developed here might be very helpful in this and similar situations.

Our scheme of functional truncations is quite general and is applicable to a variety of particular cases, including LPA, DE and BMW equations. As a first step, we have noted that it works fine for the LPA equation, comparing the results with those obtained by the purely numerical solution. Subsequently, the critical exponents of the new equation of [10] (obtained at the first order of truncation for the effective action within the new scheme considered there) have been determined with a high accuracy. The state-of-the-art values obtainable from this equation have not been reported yet. One of the aims of our current study is to fill this gap.

Our paper is organized as follows. The Wetterich equation is briefly reviewed in section 2. In section 3, a new scheme of functional truncations is introduced for the solution of truncated RG flow equations, including the BMW and DE equations, and those ones recently derived in [10] and summarized in appendix A. This scheme is tested in the LPA case in section 4 and further (in section 5) applied to the equations of [10] as an example, evaluating the critical exponents and the two-point correlation function. The summary and outlook are given in section 6. The details of the computation algorithms are provided in the Appendices B–E.

2. The Wetterich equation

We consider the Wetterich exact RG equation [6, 9]

$$\frac{\partial}{\partial k}\Gamma_k[\phi] = \frac{1}{2}\mathrm{Tr}\left\{\left[\Gamma_k^{(2)}[\phi] + R_k\right]^{-1}\frac{\partial}{\partial k}R_k\right\}, \tag{1}$$

for the effective average action $\Gamma_k[\phi]$ in presence of the running infrared cut-off scale k and external sources. It contains also the upper (ultraviolet) cut-off at $|\,\mathbf{q}\,| = \Lambda$ in the space of the wave vectors $\mathbf{q}$. For the $O(N)$ model, $\Gamma_k[\phi]$ depends on the averaged order parameter $\phi(\mathbf{x})$ (which depends on the external sources $J(\mathbf{x})$) with components $\phi_j(\mathbf{x})$, where $j = 1,\ldots,N$. In wave-vector space, the quantity $\Gamma_k^{(2)}[\phi]$ is a matrix with elements

$$\left(\Gamma_k^{(2)}\right)_{ij}(\mathbf{q},\mathbf{q}') = \frac{\delta^2\,\Gamma_k[\phi]}{\delta\phi_i(-\mathbf{q})\,\delta\phi_j(\mathbf{q}')}\,. \tag{2}$$

Using discrete wave vectors, as in [10], the cut-off function R_k is represented as

$$R_{k,ij}(\mathbf{q},\mathbf{q}') = R_k(q)\,\delta_{ij}\,\delta_{\mathbf{q},\mathbf{q}'}\,. \tag{3}$$

An appropriate choice for application in critical phenomena is [9, 14, 15]

$$R_k(q) = \frac{\alpha Z_k q^2}{e^{q^2/k^2}-1}\,, \tag{4}$$

where Z_k is a renormalization constant and α is an optimization parameter. There are also other forms of the cut-off function $R_k(q)$ possible, as, e.g. those ones considered in [11, 19]. In this paper, we have limited our choice to (4) for simplicity.

3. Functional truncations

Closed approximate RG flow equations can, in principle, be solved purely numerically. However, we are looking here for appropriate semi-analytic approximations, called functional truncations (as introduced in section 1), which would allow to obtain accurate results with smaller

computational effort and would also be generally applicable for the solution of the nonperturbative RG equations. For applications to critical phenomena, these equations are usually transformed into a dimensionless form, containing the dimensionless potential $u_k(\tilde{\rho})$. The dimensionless quantities $u_k(\tilde{\rho})$ and $\tilde{\rho}$ are properly defined in appendix A in relation to the recent truncated RG flow equations of [10] for the Ising universality class, considered throughout this paper. These quantities are commonly used also in other known truncation schemes for the effective average action. The RG flow equations can generally contain additional functions of $\tilde{\rho}$. The scheme of [10] and the BMW scheme include also the quantities that depend on the dimensionless momentum $\tilde{p} = p/k$ (p being the momentum) or $y = \tilde{p}^2$. The momentum dependence is represented by the function $f_k(\tilde{\rho}; y)$ in the equations of [10] (see appendix A) and by the function $\tilde{Y}_k(\tilde{p}, \tilde{\rho})$, having the same meaning as $f_k(\tilde{\rho}; y) - 1$, in the first-order approximation of the BMW scheme [18].

The RG flow equations emerging at a given order of the DE are traditionally solved either purely numerically [19] or by certain functional truncations, i.e. truncated expansions in powers of $\tilde{\rho} - \tilde{\rho}^*$ [9], where $\tilde{\rho}^*$ corresponds to the minimum of $u_k(\tilde{\rho})$. We propose a different expansion. For the equations of [10] and those of the BMW scheme (where we substitute $\tilde{Y}_k(\tilde{p}, \tilde{\rho}) \to f_k(\tilde{\rho}; y) - 1$), our new method of functional truncations is implemented via the representation

$$u_k(\tilde{\rho}) - u_k(0) = \bar{u}_k(s) = (1-s)^{-\mu}\, \hat{u}_k(s)\,, \tag{5}$$

$$f_k(\tilde{\rho}; y) = \bar{f}_k(s; y)\,, \tag{6}$$

where $s = \tilde{\rho}/(\tilde{\rho}_0 + \tilde{\rho})$ and $\mu = d/(d - 2 + \eta)$, with the following truncated expansions

$$\hat{u}_k(s) = \sum_{m=1}^{n} u_{m,k}\, s^m\,, \tag{7}$$

$$\bar{f}_k(s; y) = \sum_{m=0}^{n'} f_{m,k}(y)\, s^m\,. \tag{8}$$

Here $\tilde{\rho}_0$ is an optimization parameter and μ is the exponent, which describes the power-law divergence of $u_k(\tilde{\rho})$, i.e. $u_k(\tilde{\rho}) \propto \tilde{\rho}^{\mu}$, given $\tilde{\rho} \to \infty$ at the fixed point. In this case, the divergence with $\mu = d/(d - 2 + \eta)$ follows from (36), where the integral is negligible at $\tilde{\rho} \to \infty$. Thus, we interpolate between the expansion in powers of $\tilde{\rho}$ at $\tilde{\rho} \to 0$ and the power-law asymptotic at $\tilde{\rho} \to \infty$. The exponent μ is adjusted to the fixed point to make this form optimal for the estimation of critical exponents. As we have found *a posteriory*, the precise large-$\tilde{\rho}$ behavior has a minor importance, so that the form used here is applicable also away from the fixed point. We have not used an exponent like μ in (6), because $f_k(\tilde{\rho}; y)$ does not diverge at $\tilde{\rho} \to \infty$. The expansions proposed here are better than those in powers of $\tilde{\rho}$ or even $\tilde{\rho} - \tilde{\rho}^*$, as regards the large-$\tilde{\rho}$ behavior. Indeed, the latter expansions suggest that both $u_k(\tilde{\rho})$ and $f_k(\tilde{\rho}; y)$ diverge as $\propto \tilde{\rho}^n$ at $\tilde{\rho} \to \infty$, where n is the order of truncation. Formally, the expansion in powers of $\tilde{\rho}$ is recovered from (5)–(8) at $\tilde{\rho}_0 \to \infty$, since $\tilde{\rho} \propto s$ holds in this case for any fixed interval of finite $\tilde{\rho}$ values. However, certain finite values of $\tilde{\rho}_0$ ensure the best convergence, so that our new expansion is certainly better than the expansion in powers of $\tilde{\rho}$. Intuitively, the advantage in using the expansion parameter s instead of $\tilde{\rho}$ or $\tilde{\rho} - \tilde{\rho}^*$ is related to the fact that s is bounded within $s \in [0, 1]$ and, therefore, it ensures a more stable behavior at relatively large values of $\tilde{\rho}$ (as compared to $\tilde{\rho}^*$), noting that $\tilde{\rho} \to \infty$ corresponds to $s \to 1$.

This method of functional truncations can be easily applied to other truncated RG flow equations (within the LPA, DE and BMW schemes) containing function(s) of $\tilde{\rho}$ (or functions of $\phi = \sqrt{2\,\rho}$, which are reducible to functions of $\tilde{\rho}$). These equations contain the potential

$u(\tilde{\rho})$, for which the expansion (7) is applicable. Other functions of $\tilde{\rho}$ can also be represented in terms of s. In particular, the dimensionless renormalization constant $z_k(\tilde{\rho})$ of the DE at the $O\left(\partial^2\right)$ order can be expanded as

$$z_k(\tilde{\rho}) = \sum_{m=0}^{n'} z_{m,k} s^m \,, \tag{9}$$

noting that $z_k(\tilde{\rho}) = f_k(\tilde{\rho};0)$ [10]. More generally, the $\tilde{\rho}$-dependent quantities (numbered by index i), which show up in the considered RG flow equations, can be represented by expansions in powers of s multiplied by $(1-s)^{\mu_i}$ with $\mu_i = 0$ in the simplest case.

In the following, we will consider the RG flow equations of [10] as a basic example. Using the new variables, introduced in equations (5) and (6), these equations (see appendix A) become

$$\frac{\partial \hat{u}_k(s)}{\partial t} = (1-s)^{\mu}\left\{-d\,\bar{u}_k(s) + (d-2+\eta(k))\,s(1-s)\,\bar{u}_k'(s)\right\} - \mathcal{L}_k(s)\,, \tag{10}$$

$$\frac{\partial \bar{f}_k(s;y)}{\partial t} = \eta(k)\bar{f}_k(s;y) + (d-2+\eta(k))\,s(1-s)\bar{f}_k'(s;y) + 2y\frac{\partial \bar{f}_k(s;y)}{\partial y} + \omega_k(s;y)\mathcal{M}_k(s) - \mathcal{F}_k(s,y)\,, \tag{11}$$

$$\eta(k) = -\bar{f}_k'(0;0)\mathcal{M}_k(0)/\tilde{\rho}_0\,, \tag{12}$$

where

$$\mathcal{L}_k(s) = \frac{K_d}{4}\left[\int_0^{\Lambda^2/k^2} \frac{y^{\frac{d}{2}-1}\zeta_k(y)dy}{\bar{\mathcal{P}}_k(s,y)} - \int_0^{\Lambda^2/k^2} \frac{y^{\frac{d}{2}-1}\zeta_k(y)dy}{\bar{\mathcal{P}}_k(0,y)}\right](1-s)^{\mu}\,, \tag{13}$$

$$\mathcal{M}_k(s) = \frac{K_d}{4}\int_0^{\Lambda^2/k^2} \frac{y^{\frac{d}{2}-1}\zeta_k(y)dy}{\bar{\mathcal{P}}_k^2(s,y)}\,, \tag{14}$$

$$\bar{w}_k(s) = (1-s)^2\,\left[(1-4s)\bar{u}_k'(s) + 2s(1-s)\,\bar{u}_k''(s)\right]/\tilde{\rho}_0\,, \tag{15}$$

$$\omega_k(s;y) = (1-s)^2\,\left[(1-4s)\bar{f}_k'(s;y) + 2s(1-s)\bar{f}_k''(s;y)\right]/\tilde{\rho}_0\,, \tag{16}$$

$$\bar{\mathcal{P}}_k(s,y) = \bar{w}_k(s) + y[\bar{f}_k(s;y) + r(y)]\,, \tag{17}$$

$$\mathcal{F}_k(s,y) = y^{-1}\left[C_k(s,y) - C_k(s,0)\right]\,, \tag{18}$$

$$C_k(s,y) = \frac{s(1-s)^3}{\tilde{\rho}_0}\tilde{K}_d \int_0^{\Lambda^2/k^2}\int_0^{\pi} \zeta_k(y_1)\,\Theta\left(\frac{\Lambda^2}{k^2} - Y\right) y_1^{\frac{d}{2}-1}\,(\sin\theta)^{d-2} \times \frac{\left(\bar{w}_k'(s) + \frac{1}{2}\left[y\bar{f}_k'(s;y) + y_1\bar{f}_k'(s;y_1) + Y\bar{f}_k'(s;Y)\right]\right)^2}{\bar{\mathcal{P}}_k(s,Y)\,\bar{\mathcal{P}}_k^2(s,y_1)}\,dy_1 d\theta\,. \tag{19}$$

Here $\zeta_k(y) = 2y^2\ r'(y) + \eta(k)\,y r(y)$ and $Y = y + y_1 + 2\ \sqrt{yy_1}\cos\theta$ are the same as in equations of appendix A with

$$r(y) = \frac{\alpha}{e^y - 1} \tag{20}$$

being the dimensionless form of the cut-off function (4). The primes denote the derivatives with respect to s, except for $r'(y) = dr/dy$.

RG flow equations for the expansion coefficients in (7) and (8) are obtained by inserting these expressions into (10) and (11) and equating terms of the expansion in powers of s. It can be easily algorithmized, as shown in appendix B. Thus, we have

$$\frac{\partial u_{i,k}}{\partial t} = -du_{i,k} + (d-2+\eta(k))\sum_{j=0}^{i-1} a_j(\mu)c_{i-j,k} - \mathcal{L}_{i,k}\,, \tag{21}$$

$$\frac{\partial f_{i,k}(y)}{\partial t} = \eta(k)f_{i,k}(y) + (d-2+\eta(k))\,[if_{i,k} - (i-1)f_{i-1,k}(y)] + 2y\frac{\partial f_{i,k}(y)}{\partial y} + \sum_{\ell=0}^{i}\omega_{\ell,k}(y)\mathcal{M}_{i-\ell,k} - \mathcal{F}_{i,k}(y)\,, \tag{22}$$

$$\eta(k) = -f_{1,k}(0)\mathcal{M}_{0,k}/\tilde{\rho}_0\,. \tag{23}$$

Here $\mathcal{L}_{i,k}$ denotes the coefficient in the expansion $\mathcal{L}_k(s) = \sum_i \mathcal{L}_{i,k}s^i$, and similarly for other quantities. In addition, $a_j(\mu)$ are the expansion coefficients of $(1-s)^\mu$ and $c_{i,k}$ are those of $s(1-s)\bar{u}_k'(s)$. Details of the computational algorithm for calculation of all these coefficients are given in appendix B. In these calculations, we have replaced the sharp upper cut-off in the integrals over y by a smooth cut-off. The shape of this cut-off is unimportant when approaching the fixed point at $k \to 0$, but its smoothness (represented by equation (52)) is more convenient for calculations.

4. The LPA tests of the method

4.1. Solutions of the LPA equation

The LPA provides an excellent test of the applicability, convergence and accuracy of our new scheme of functional truncations, because the LPA equation can be solved very accurately by a purely numerical method for comparison. Such a numerical method is considered in appendix C. Note that the LPA equation is obtained from the equations of [10] (reviewed in appendix A) by setting $\eta(k) \equiv 0$ and $f_k(\tilde{\rho}; y) \equiv 1$. It is a well-known approximation [9]. Exactly the same LPA equation shows up as a zeroth-order approximation in the DE and BMW schemes, as well. Hence, the LPA equation can be approximately solved by our method of functional truncations, formally setting $n' = 0$ in (8), as well as $\bar{f}_k(s; y) = f_{0,k}(y) \equiv 1$ and $\eta(k) \equiv 0$. In this case, we only need to apply equation (21) with $\eta(k) \equiv 0$ and the computational algorithm (appendix B) for the coefficients in this equation.

In this paper, all results have been obtained by a direct integration of the RG flow equations. The fixed point is reached by adjusting the initial condition iteratively, and the critical exponents are determined from the RG flow at and near the critical surface, as described in appendix D. Generally, we consider the critical exponents ν, ω and η, the latter one being zero in the LPA. The critical exponent η describes the $\propto k^{-2+\eta}$ divergence of the critical two-point correlation function, as well as the $\propto k^{-\eta}$ divergence of the renormalization constant Z_k on the critical surface at $k \to 0$. The critical exponent ν describes the $\propto |\,\tau\,|^{-\nu}$ divergence of the correlation length at $\tau \to 0$, where τ is the deviation from the critical temperature. It describes also the $\propto k^{-1/\nu}$ deviation of the RG flow from the fixed point at small k values so close to critical surface that this deviation is small. The critical exponent ω describes corrections to scaling, as well as the $\propto k^{\omega}$ distance of the RG flow from the fixed point on the critical

surface at $k \to 0$. The details of the extraction of these critical exponents from the RG flow are given in appendix D.

For the purely numerical solution (appendix C), a certain grid of $\tilde{\rho}$ values was used, where the origin is at $\tilde{\rho} = 0$, the next grid point is at $\tilde{\rho} = \tilde{\rho}_1$, and each next step size is by a factor $1 + \varepsilon$ larger than the previous one. The grid parameters ε and $\tilde{\rho}_1$ essentially influence the critical exponents extracted from this solution. Therefore, an extrapolation to $\tilde{\rho}_1 \to 0$ and $\varepsilon \to 0$ has been performed, using the data for $\varepsilon = 0.025$, 0.0125 and 0.00625 with $\tilde{\rho}_1 = 0.1\ \varepsilon$, to obtain very accurate results. In other cases, one set of step sizes was sufficient for the desired accuracy. The details about the difference scheme, grids and step sizes, used in our functional truncation scheme, are provided in appendix E.

It is interesting to note that the results (the potential and the critical exponents) of our functional truncations are independent of $\tilde{\rho}_0$ at $n = 3$ (and only at $n = 3$) in three dimensions in the LPA case of $n' = 0$, as it has been verified numerically. This fact has the following explanation. In the LPA case at $d = 3$ we have $\eta = 0$ and $\mu = d/(d-2) = 3$, so that the truncated expansion (5) at $n = 3$ reduces to the third-order polynomial in $\tilde{\rho}$, i.e. $(1-s)^{-3}\left(u_{1,k}s + u_{2,k}s^2 + u_{3,k}s^3\right) = a_{1,k}\tilde{\rho} + a_{2,k}\tilde{\rho}^2 + a_{3,k}\tilde{\rho}^3$, where $a_{1,k} = u_{1,k}/\tilde{\rho}_0$, $a_{2,k} = (2u_{1,k} + u_{2,k})/\tilde{\rho}_0^2$ and $a_{3,k} = (u_{1,k} + u_{2,k} + u_{3,k})/\tilde{\rho}_0^3$. Thus, the truncated expansion (7) at $n = 3$ appears to be exactly equivalent to the truncated at the third order expansion in powers of $\tilde{\rho}$. Such equivalence is possible only at $n = 3$ because only in this case the number of parameters $u_{m,k}$ is the same as the number of the corresponding parameters $a_{m,k}$, noting that $(1-s)^{-3}\sum_{m=0}^{n} u_{m,k}s^m$ is not equal to a truncated polynomial of $\tilde{\rho}$ at $n > 3$. Considering the expansion in powers of $\tilde{\rho}$ with $a_{1,k}$, $a_{2,k}$ and $a_{3,k}$ as independent parameters, the RG flow equations for these parameters and the results do not contain $\tilde{\rho}_0$. The above equivalence means that (7) at $n = 3$ also provide results, which are independent of $\tilde{\rho}_0$ in the actual case of LPA.

In fact, $\tilde{\rho}_0$ serves as a good optimization parameter for $n > 3$.

4.2. The convergence test for the potential

We have tested the convergence of the shifted fixed-point potential $u(\tilde{\rho}) = u_k(\tilde{\rho}) - u_k(0)$ at $k \to 0$, obtained by the functional truncation (7) in the LPA case at $d = 3$ with $\alpha = 2$ in (20) as an example. We have chosen either $\alpha = 2$ or $\alpha = 5$ in most of our tests, since $\alpha = 5$ appears to be not far from the optimal value in the determination of the LPA critical exponents, whereas $\alpha = 2$ is a nearly optimal choice beyond the LPA.

One could hope to reach the convergence within $\tilde{\rho} \in [0, \infty[$ because $s \in [0, 1]$. However, considering $n \leqslant 13$, we have observed a convergence only within a finite $\tilde{\rho}$ interval, which depends on the optimization parameter $\tilde{\rho}_0$. We have tested $\tilde{\rho}_0 = 0.4$, $\tilde{\rho}_0 = 0.5$ and $\tilde{\rho}_0 = 0.6$ and have observed that the convergence improves with decreasing of $\tilde{\rho}_0$ within this range of values. For significantly smaller $\tilde{\rho}_0$ values, however, the RG flow becomes unstable in some sense, in such a way that we could not get the fixed point from the initial conditions we used. The results for $\tilde{\rho}_0 = 0.4, 0.5, 0.6$ at the truncation orders $n = 4, 7, 10, 13$ are shown in figure 1, where the purely numerical solution is also shown for comparison. Apparently, the series of functional truncations converge accurately to the purely numerical solution within about $\tilde{\rho} < 0.3$ for $\tilde{\rho}_0 = 0.4$ and within a narrower $\tilde{\rho}$ interval for $\tilde{\rho}_0 = 0.5$ and $\tilde{\rho}_0 = 0.6$. The results for $n = 13$ are collected and compared with the purely numerical solution at the grid parameters $\varepsilon = 0.00625$ and $\varepsilon = 0.0125$ in figure 2. Obviously, the grid step size has a tiny influence in this case. As we can see, our functional truncations reproduce very accurately the shape of the potential around its minimum at $\tilde{\rho} = \tilde{\rho}^* \approx 0.05$. Since the best results have been obtained at $\tilde{\rho}_0 = 0.4$, we have used this value in most of the following calculations.

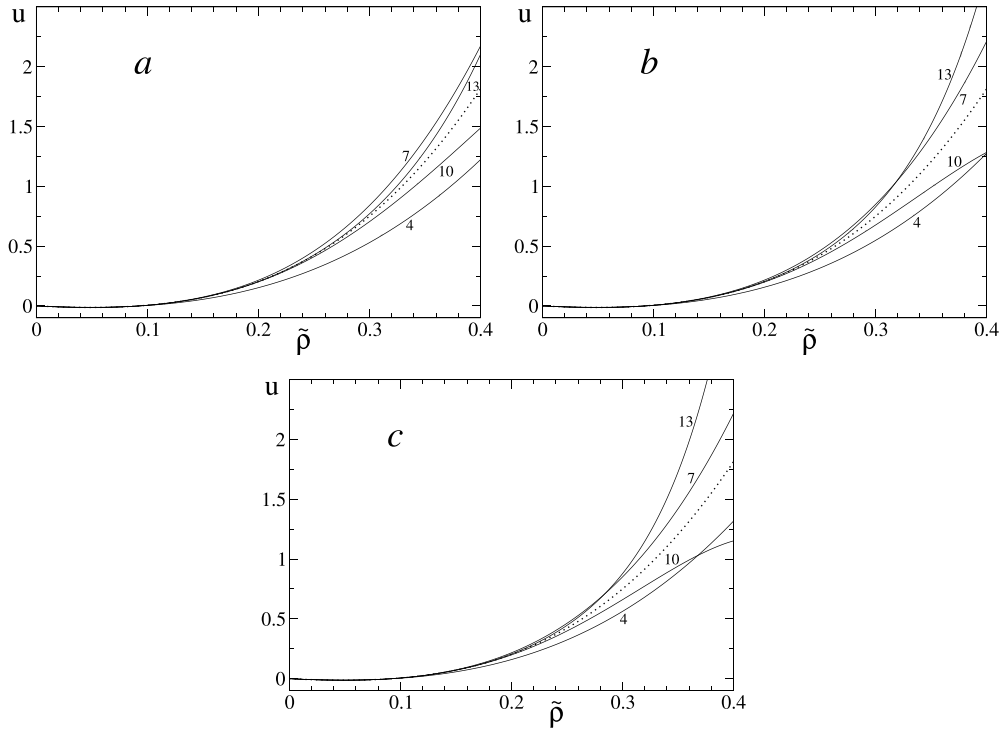

Figure 1. The shifted fixed-point potential $u(\tilde{\rho}) = u_k(\tilde{\rho}) - u_k(0)$ for three values of the parameter $\tilde{\rho}$, i.e. $\tilde{\rho}_0 = 0.4$ (*a*), $\tilde{\rho}_0 = 0.5$ (*b*) and $\tilde{\rho}_0 = 0.6$ (*c*) at different truncation orders n in (7). The values of n are indicated at the corresponding solid curves. The result of the purely numerical solution on the finest grid with $\varepsilon = 0.006\,25$ is shown in each case (*a, b, c*) by the dotted line for comparison.

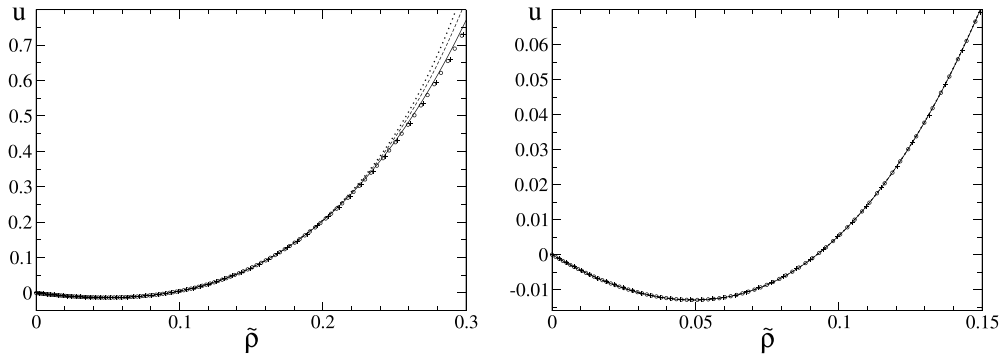

Figure 2. Left: The shifted fixed-point potential $u(\tilde{\rho}) = u_k(\tilde{\rho}) - u_k(0)$ for $\tilde{\rho}_0 = 0.4$ (solid curve), $\tilde{\rho}_0 = 0.5$ (dashed curve) and $\tilde{\rho}_0 = 0.6$ (dotted curve) at $n = 13$. The results of the purely numerical solution on the grids with $\varepsilon = 0.006\,25$ and $\varepsilon = 0.0125$ are shown by circles and pluses, respectively. Right: the same figure zoomed to show the shape of the potential around its minimum.

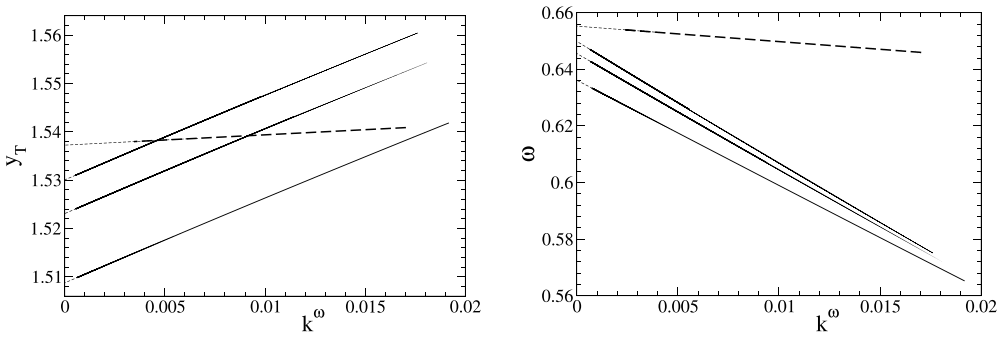

Figure 3. The running exponents y_T (left) and ω (right) at $\alpha = 5$ depending on k^ω. The results of the purely numerical solution are shown by solid lines, whereas those of the functional truncation at $n = 13$—by dashed lines. The tiny dashed lines represent the linear extrapolation, used for estimation of the asymptotic exponents.

In section 4.3, we demonstrate that our functional truncations provide also very accurate values of the critical exponents. Hence, we can judge that accurate results for the potential within $\tilde{\rho} \in [0, C\tilde{\rho}^*]$, where C is a large enough constant, ensure accurate critical exponents, the relatively large inaccuracy within $\tilde{\rho} > C\tilde{\rho}^*$ playing almost no role. This conclusion is supported also by the purely numerical solutions with different values of $\tilde{\rho}_{\max}$, where $\tilde{\rho}_{\max}$ is the maximal $\tilde{\rho}$ value on the grid: routinely, we have used $\tilde{\rho}_{\max} = 2$, but $\tilde{\rho}_{\max} = 5$ gave precisely (with 16 digits accuracy) the same results.

4.3. The convergence of the critical exponents

Here we consider the critical exponents $y_T = 1/\nu$ and ω in three dimensions. The exponent y_T describes the $\sim k^{-y_T}$ deviations of the RG flow from the critical surface, whereas the correction-to-scaling exponent ω describes the $\sim k^\omega$ rate of convergence to the fixed point on the critical surface. We have extracted the running (effective) k-dependent exponents from the RG flow, as described in appendix D. The running exponent $\omega(k)$ is almost perfectly linear function of k^ω at small k, where ω is the self-consistently determined asymptotic exponent. It means that the leading corrections to scaling at the critical temperature are described by the exponent ω, but the subleading ones predominantly by the exponent $2\,\omega$, which comes from the second-order correction $\sim (k^\omega)^2 = k^{2\,\omega}$. Deviations along the critical surface of the effective potential from its value at the critical point scale like k^ω. Because practically we estimate the running exponent $y_T(k)$ as a function of this potential, this estimate appears as linear function of k^ω in the vicinity of the critical point. Its actual value is then obtained in the limit $k \to 0$.

These exponents for $\alpha = 5$ in (20), as an example, are plotted in figure 3. The results of the purely numerical solution (solid lines) are remarkably influenced by the grid parameter ε, whereas those of the functional truncation at $n = 13$ are quite unambiguous. The asymptotic exponents are obtained by a linear extrapolation (tiny dashed lines). Very accurate purely numerical asymptotic estimates are obtained by a quadratic fit of the results over finite values of ε, as shown in figure 4 for $\alpha = 2$ and $\alpha = 5$. The extrapolated to $\varepsilon \to 0$ values in figure 4 are very close to those provided by the functional truncations at $n = 13$, which are indicated by horizontal dotted lines.

The convergence test for the critical exponents ν and ω depending on the truncation order n in our scheme has been performed for $\alpha = 2$ at $\tilde{\rho}_0 = 0.4$ and $\tilde{\rho}_0 = 0.5$. The results are presented

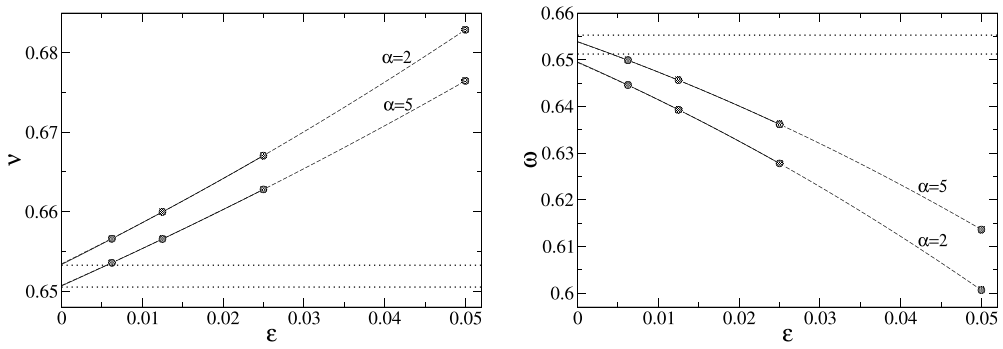

Figure 4. The critical exponents ν (left) and ω (right) of the purely numerical solution depending on the grid parameter ε at $\alpha = 2$ and $\alpha = 5$, as indicated at the corresponding curves. Quadratic fits over three smallest ε values are shown by solid curves, whereas those over three largest ε values are shown by dashed lines for comparison. The horizontal dotted lines show the corresponding values of the functional truncation at $n = 13$.

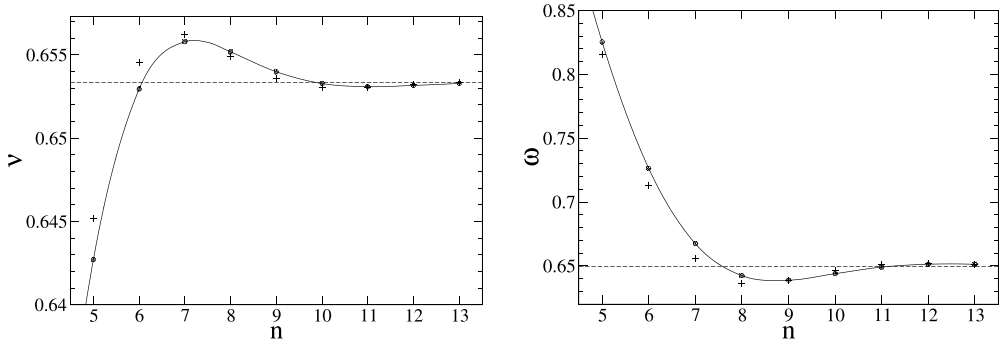

Figure 5. The critical exponents ν (left) and ω (right) for $\alpha = 2$ at $\tilde{\rho}_0 = 0.4$ (circles) and $\tilde{\rho}_0 = 0.5$ (pluses) depending on the truncation order n in (7). The values of the purely numerical solution are shown by horizontal dashed lines.

in figure 5. A good convergence to the values of the purely numerical solution (horizontal dashed lines) is evident for both ν (left) and ω (right). Moreover, a convergence to the same value is observed at $\tilde{\rho}_0 = 0.4$ (circles) and $\tilde{\rho}_0 = 0.5$ (pluses).

The values of the critical exponents depend on the parameter α, and it is commonly accepted to apply the principle of minimal sensitivity (PMS) [14, 15] to find the optimal value of α. Practically, it means that we plot the critical exponents as functions of α and find an extremum point, as shown in figure 6. From these plots we find the PMS values

$$\nu_{\rm PMS} = 0.650601(10), \tag{24}$$

$$\omega_{\rm PMS} = 0.654115(30), \tag{25}$$

of the purely numerical solution, which have to be compared with $\nu_{\rm PMS} = 0.6504475(23)$ and $\omega_{\rm PMS} = 0.655301(11)$ of the functional truncation scheme at $n = 13$. The error bars indicated here refer to the numerical errors due to the integration step sizes, deviations from a perfect scaling, etc not including the truncation errors. Comparing these results, we conclude that the truncation error at $n = 13$ is ≈ 0.00015 for ν and ≈ 0.0012 for ω.

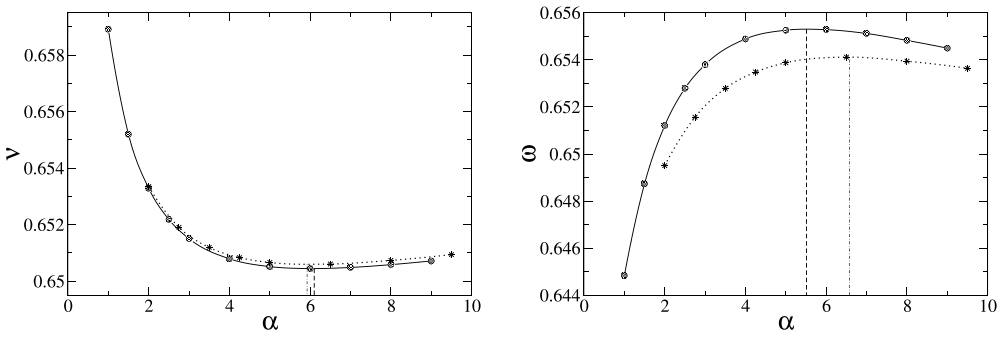

Figure 6. The critical exponents ν (left) and ω (right) depending on the optimization parameter α for the functional truncation at $n=13$ in (7) (solid spline curves) and for the purely numerical solution (dotted spline curves). The PMS values correspond to the extremum points of these curves, as indicated by the vertical dashed and dot-dashed lines.

Here we have used (24) and (25) as very accurate reference values for the LPA exponents at a specific cut-off function (20). This ω value matches the value 0.6541 reported for (20) in table III of [19]. Moreover, our ν value perfectly matches the estimate $\nu=0.651(1)$ cited in [11]. Note, however, that the error bars of the latter case include variations due to different cut-off functions.

The values of ν and ω discussed here are close to the LPA estimates $\nu=0.649562$ and $\omega=0.655746$, obtained in [16] by the traditional truncated expansion in powers of $\tilde{\rho}-\tilde{\rho}^*$, where $\tilde{\rho}^*$ corresponds to the minimum of the potential. The latter values, however, refer to a cut-off function different from (20) $r(y)=\left(\frac{1}{y}-1\right)\theta(1-y)$, which is optimal for the LPA [16]. As pointed out in [15], this cut-off function is not applicable for a refined estimation within the DE of the $O\left(\partial^4\right)$ order and higher orders because it is not smooth. Nevertheless, it ensures a very fast convergence of the traditional expansion within the LPA [16], which is even faster than that one provided by (7) and shown in figure 5. At the same time, the expansion in powers of $\tilde{\rho}$, also considered in [16], provides worse results than those in figure 5. The convergence properties essentially depend on the cut-off function [16], therefore this comparison is not fully conclusive. Apparently, our new functional truncations are advantageous in refined estimations beyond the LPA. The LPA results of the traditional functional truncations for η, ν and ω have been obtained in [16], whereas the corresponding DE results have been reported in [14, 15] for η and ν only. Our new functional truncations work well for a refined estimation of all these exponents, including ω, as further shown in section 5.2.

5. The solution of the new truncated equation

5.1. The convergence of $f_k(\tilde{\rho};y)$

We have applied our method of functional truncations to the case of $n'>0$ in (8) in three dimensions. Here we consider the convergence of $f_k(\tilde{\rho};y)$ at the fixed point, setting $n=13$ in (7) and choosing $\tilde{\rho}_0=0.4$. The results at four different values of $\tilde{\rho}$ are shown in figure 7. Considering $n'\leqslant 10$, we observe a convergence within the range of $\tilde{\rho}<0.15$. This is the same range around the minimum of the potential seen in figure 2(right). Apparently, the convergence

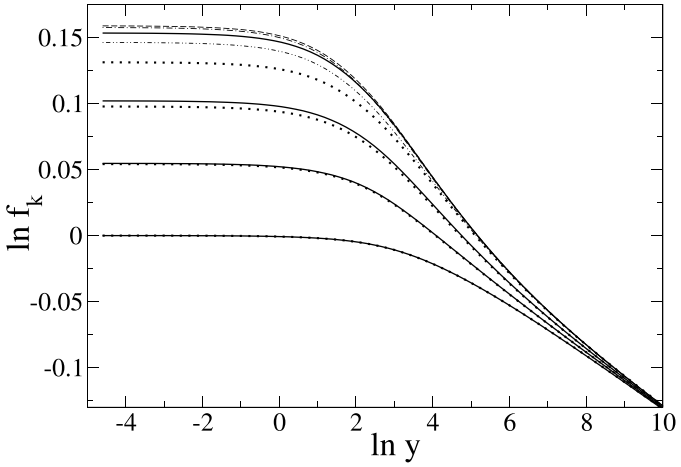

Figure 7. The convergence test for the function $f_k(\tilde{\rho};y)$ at $n=13$ in (7). The results for $n'=6$ and $n'=10$ in (8) are shown by the dotted and the solid curves, respectively. From the bottom to the top, these curves correspond to $\tilde{\rho}=0$, $\tilde{\rho}=0.05$, $\tilde{\rho}=0.1$ and $\tilde{\rho}=0.15$. The dot-dot-dashed, dot-dashed and dashed curves represent the results for $n'=7$, $n'=8$ and $n'=9$, respectively, at $\tilde{\rho}=0.15$.

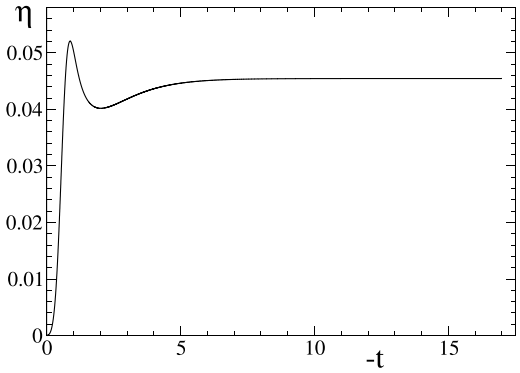

Figure 8. The running exponent $\eta(k)$ on the critical surface for $\alpha=2$, evaluated at the truncation orders $n=13$ and $n'=10$.

of $f_k(\tilde{\rho};y)$ within $\tilde{\rho}<0.15$ is sufficient for a rapid convergence of the critical exponents, as we can judge from the results of the following subsection.

5.2. The critical exponents

Here we consider the critical exponents, starting with η, which is directly estimated as the fixed-point value of the running exponent $\eta(k)$. It has to be noted that the exponent μ in (5) contains a constant (fixed-point) value of η, which is first obtained by a trial calculation, as described in appendix D. The parameter $\tilde{\rho}_0=0.4$ is used in all the following calculations at $d=3$. The running exponent $\eta(k)$ on the critical surface, evaluated at the truncation orders $n=13$ and $n'=10$, is shown in figure 8 for illustration at $\alpha=2$. In this case, $\eta(k)$ is almost

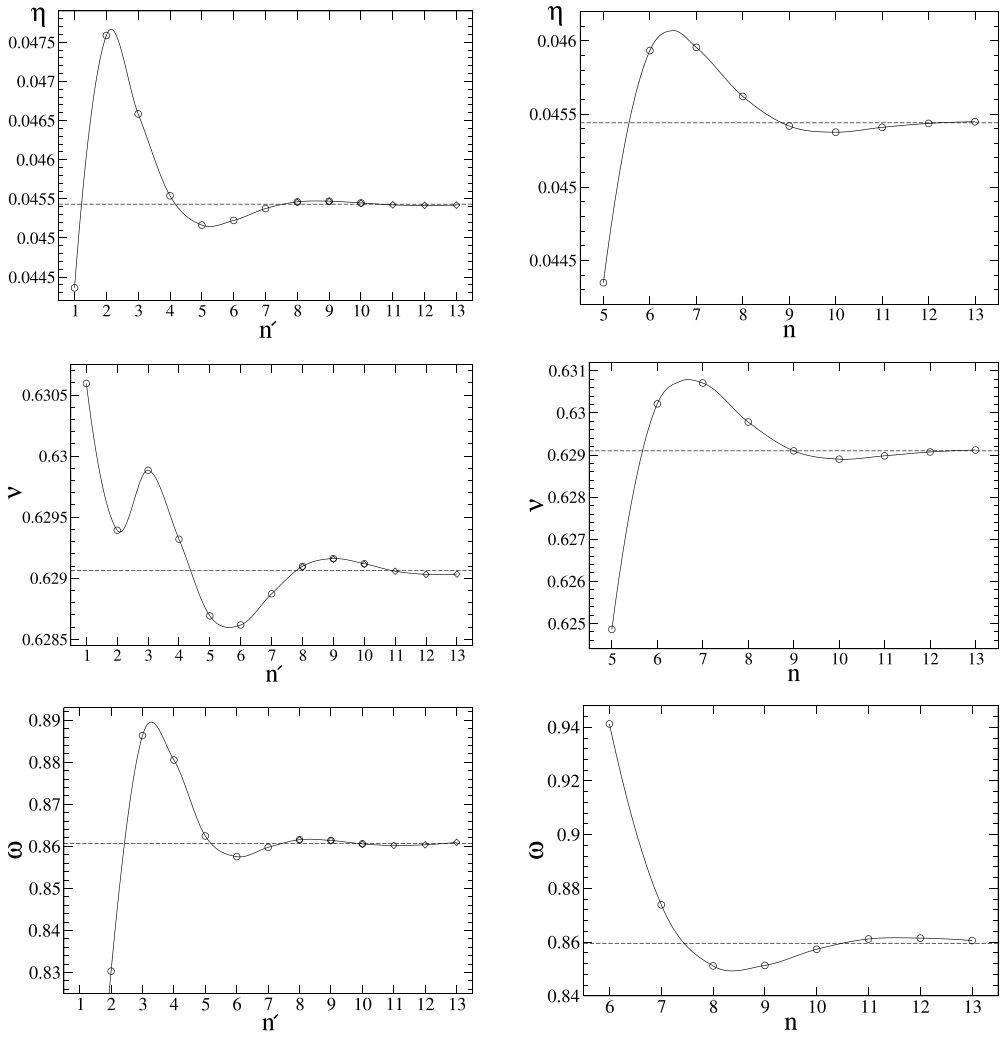

Figure 9. The critical exponents η (top), ν (middle) and ω (bottom) depending on $n^{'}$ at $n = 13$ (left), and depending on n at $n' = 10$ (right), where n and $n^{'}$ are the truncation orders in (7) and (8). Circles and rhombs represent the results obtained at standard and rough grid step sizes (see appendix E), respectively. The horizontal dashed lines indicate approximate values to which the critical exponents apparently converge.

constant at large enough values of $-t$. To minimize the numerical error, we have evaluated η at such a value of t, at which $\mid \partial\eta(k)/\partial t \mid$ is minimal.

Further on, we have tested the convergence of the critical exponents in two ways. First, we have fixed the maximal used value on n, i.e. $n = 13$ in the expansion of the potential (7) to see how the results are influenced by the truncation in (8). Second, we have fixed $n' = 10$ in (8) and have examined the influence of the truncation in (7). We have performed these tests for $\alpha = 2$. This value appeared to be nearly optimal for the determination of the critical exponents η and ω and also not too far from optimal for ν. The convergence of η, ν and ω has been tested, as shown in figure 9.

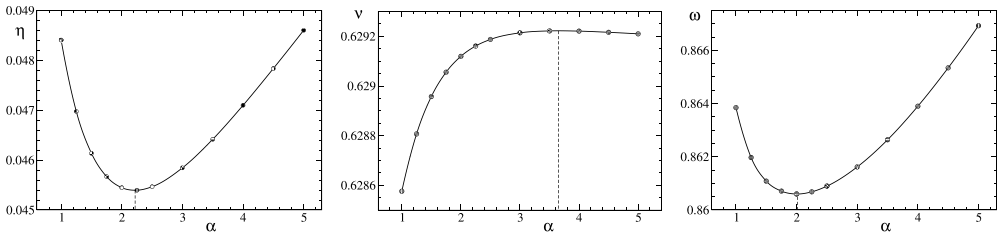

Figure 10. The critical exponents η (left), ν (middle) and ω (right) depending on the optimization parameter α for the functional truncation at $n=13$, $n'=10$ in (7) and (8). The PMS values correspond to the extremum points, indicated by vertical dashed lines.

For the tests with $n=13$, we have performed calculations up to $n'=10$ with certain standard (used in most of the cases) grid step sizes. Additional calculations for $n'\in[8,13]$ have been performed with twice increased step sizes. Such an extension up to $n'=13$ allows us to see the convergence much better, while the increased step sizes helped to speed up these calculations without any essential loss of the accuracy—see the overlapping values at $n'=8,9,10$ in figure 9.

We conclude from these tests that the truncation at $n=13$ and $n'=10$ gives already quite accurate results. Therefore, we have extended the calculations at these truncation orders to include several values of the optimization parameter α, allowing to find the PMS values of the critical exponents. As usual, these are determined as the extremum values of the corresponding plots, shown in figure 10. Finally, we have evaluated from these plots the critical exponents of the new truncated equation introduced in [10] in three dimensions with the cut-off function (20). These exponents are

$$\eta=0.0454(1),\quad \nu=0.6292(2),\quad \omega=0.8606(30). \tag{26}$$

The error bars include the functional truncation errors, as well as relatively smaller numerical errors of different origin. These values appear to be quite close to those reported in [11, 19] for the DE at the $O\left(\partial^2\right)$ order, i.e. $\eta=0.0449(6)$, $\nu=0.6278(3)$ and $\omega\approx 0.8702$. For comparison, the conformal bootstrap method gives $\eta=0.0362978(20)$ and $\nu=0.629971(4)$ [33].

The exact solution of the Wetterich equation would provide universal critical exponents, which are independent on the optimization parameter α. Therefore an expected property of a good truncation scheme for the effective action is that the estimated critical exponents become less dependent on α with increasing of the truncation order. Concerning the scheme of [10], tested here in detail, currently we can compare only its zeroth-order approximation, which is the LPA, with the the first-order truncation. In this case, it is meaningful to compare the α-dependence of the critical exponents ν and ω in figures 6 and 10, respectively. As we can see, the magnitude of variations of ω within $\alpha\in[1,5]$ in figure 10 is somewhat smaller than that in figure 6. The variations of ν in figure 10 are by an order of magnitude smaller than those in figure 6. It gives a good sign that the above mentioned expected property of a weaker α-dependence at higher truncation orders could be satisfied for the truncation scheme of [10], at least for the critical exponent ν.

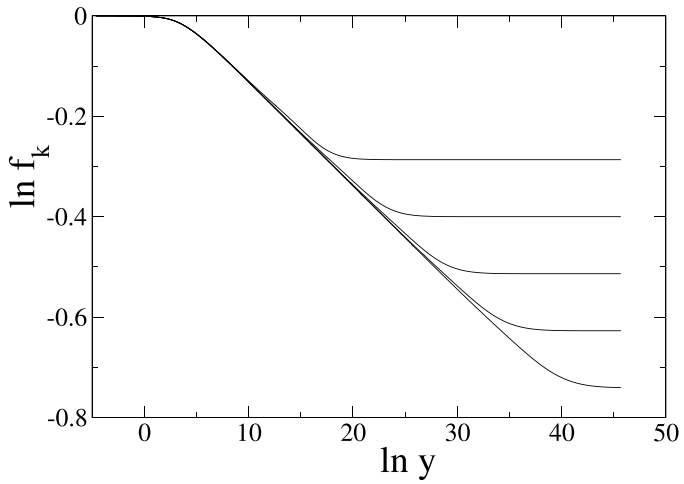

Figure 11. The $\ln f_k(0;y)$ vs $\ln y$ plots at criticality in three dimensions, calculated on a finite grid for $\alpha = 2$, using the functional truncations with $n = 13$ and $n' = 10$. From top to bottom, the curves correspond to $t = -7, -9.5, -12, -14.5$ and -17.

5.3. The two-point correlation function

Here we consider the critical two-point correlation function $G_k(\mathbf{q})$. According to [10] (see equation (94) in [10]),

$$G_k(\mathbf{q}) \approx \frac{1}{Z_k q^2 f_k(0;y)} = \frac{q^{-2+\eta}}{k^\eta Z_k y^{\eta/2} f_k(0;y)} \tag{27}$$

holds at small k and large $y = q^2/k^2$, noting that $Z_k \propto k^{-\eta}$ holds at $k \to 0$. Hence, the deviations of $G_k(\mathbf{q})$ from the asymptotic $\propto q^{-2+\eta}$ behavior are determined by the deviations of $f_k(0;y)$ from the $f_k(0;y) \propto y^{-\eta/2}$ behavior at large y. These are corrections to scaling due to the upper cut-off at $q \sim \Lambda$, or $y \sim \Lambda^2/k^2$. Hence, the smaller is k or $t = \ln(k/\Lambda)$, the larger are y values at which we observe the large-y deviations from the $f_k(0;y) \propto y^{-\eta/2}$ behavior. This can be seen in figure 11.

In fact, there is a crossover from $f_k(0;y) \propto y^{-\eta/2}$ to $f_k(0;y) \approx const$ behavior at $y \sim 1/k^2 = e^{-2t}$, noting that we have used a smooth cut-off (52) and $\Lambda = 1$. The small-y behavior, seen in figure 11, is a different effect due to the lower or infrared cut-off.

While the asymptotic slope of the $\ln f_k(0;y)$ vs $\ln y$ plot in figure 11 is given by the exponent $-\eta/2$, small deviations from the asymptotic straight line are $\sim q^\omega \propto y^{\omega/2}$, where ω is the correction-to-scaling exponent. These relations hold for our solutions with numerical errors, which decrease with reduction of the grid step sizes.

6. Summary and outlook

In this paper, a new approach of functional truncations for the solution of the non-perturbative RG equations has been developed and tested (sections 3–5). The new method allows to find accurate values of the critical exponents η, ν and also ω for the given equation. The accurate

estimation of them beyond the LPA could be an advantage, compared to the traditional expansions in powers of $\tilde{\rho} - \tilde{\rho}^*$. It becomes most apparent in the determination of the critical exponent ω. The errors of our new method at the $n = 13$ order of truncation appear to be as small as $\approx 0.000\,15$ for ν and ≈ 0.0012 for ω in the case of LPA. The critical exponents $\eta = 0.0454(1)$, $\nu = 0.6292(2)$ and $\omega = 0.8606(30)$ have been found for the new truncated (at the first order) equation recently derived in [10].

The new scheme of functional truncations has been proposed as an alternative to the traditional functional truncations, as well as to the purely numerical solutions. As mentioned in section 1, our method might be very helpful in the cases, where the purely numerical approach suffers from instability problems. In particular, it could be applied to the refined RG flow equations within the BMW scheme, considered in appendix B of [18]. As pointed out there, no solution of these refined equations has been found due to the problems of numerical instability. The derivatives with respect to ϕ, contained in these equations, can be the only source of numerical instabilities, when one tries to represent these derivatives by finite differences. Obviously, this problem would not show up in the semi-analytic approach developed here, because the ϕ-dependence (which is reducible to the $\tilde{\rho}$-dependence via $\phi = \sqrt{2\,\rho}$ and $\tilde{\rho} = Z_k k^{2-d}\rho$, and then to the s-dependence via equations of section 3) would be described in a purely analytic form.

In this paper, we have focused on the application of our new scheme of functional truncations to the equations of LPA and those derived in [10]. The developments in this direction are interesting because the equations of [10], like those of the BMW scheme [18], preserve the full momentum dependence. It is important in applications, where the high-momenta (large-q) behavior of the correlation functions is crucial. Such cases have been discussed in [18].

Concerning the critical exponents, the usual argument is that the high-momenta behavior is not important here. Thus, one can judge in favor of the DE scheme of [19], as it can be relatively easily (e.g. as compared the BMW scheme) extended and has been already extended up to the $O(\partial^6)$ order [11, 19], giving very accurate results. We stress that our new method of functional truncations is useful within the DE scheme, too. It can speed up the calculations, as compared to the numerical solution on a grid of $\tilde{\rho}$ values.

Apparently, there are still some problems with the DE. In particular, the DE solutions obtained in [11, 19] for the 3D Ising universality class ($N = 1$) do not satisfy the expected property of a weaker dependence on the optimization parameter α for higher truncation orders—see figure 1 in [11] and figure 2 in [19]. Recall that this property for the scheme of [10], has been discussed in section 5.2. Intuitively, the strengthening of the α-dependence with increasing the order $O\left(\partial^{2m}\right)$ observed in [11, 19] should lead to problems at large enough m. Indeed, at such α-dependence, the overall accuracy of the solution would decrease for large m, because no simultaneous convergence of η, ν and ω is observed at any given value of α. Although the DE values of the critical exponents η and ν in [11, 19] show a very good convergence to the 'exact' values of the conformal bootstrap method [33], the results for ω are less convincing. Indeed, the value of ω at the $O\left(\partial^6\right)$ order has not been reported in [19] along with those for η and ν, although all these exponents are determined simultaneously from the RG flow. It leads us to reckoning that there are some problems with ω at the $O\left(\partial^6\right)$ order of the DE, and the reason for this might be the violation of the expected property discussed above. Therefore, it would be very important to extend the BMW scheme [18] and the scheme of [10] beyond the first order of truncation to see whether or not these schemes will give the expected weakening of the α-dependence, as well as to check the value of ω to which the results converge. This is interesting in view of the recent discussion in [34], allowing that ω could be smaller than usually expected. Our currently proposed semi-analytic approximations can help in making the above mentioned extensions feasible.

In our current study, the critical exponents have been determined in a very straightforward way by the integration of the RG flow equations. Alternatively, one could try to find the fixed point and the critical exponents in a more efficient (faster) way, e. g, by certain iterations like those used in [10]. However, the example calculations in [10] are based on the simplest approximations. We stress that the development of such fast iterative methods within the actual refined scheme of functional truncations is a challenge for future work. If such methods would be found, then the current results could serve for their validation, because the actual method is straightforward and reliable.

Data availability statement

The data that support the findings of this study are available upon reasonable request from the authors.

Acknowledgments

The authors acknowledge the use of resources provided by the Latvian Grid Infrastructure and High Performance Computing Centre of Riga Technical University. J K acknowledges the support from the Science Support Fund of Riga Technical University. R M acknowledges the support from the NSERC and CRC program.

Appendix A. The recent truncation scheme of [10] for the effective average action

We test our method of functional truncations on the widely known LPA equation, as well as on the recent equations of [10] as an example. This is a convenient example because the LPA shows up as a zeroth order approximation of these equations and the DE at the $O(\partial^2)$ is their small-$\mathbf{q}$ approximation [10]. Therefore, these equations are briefly reviewed below.

Following [10], we consider the effective average action of the $O(N)$ symmetric model at $N=1$ (which belongs to Ising universality class) having the general form

$$\begin{aligned}\Gamma_k[\phi] = \int \Bigg(& U_k(\rho(\mathbf{x})) \\ & + V^{-1} \sum_{\mathbf{q}_1,\mathbf{q}_2} \left[\theta_k^{(1)}(\rho(\mathbf{x});\mathbf{q}_1) + \theta_k^{(2)}(\rho(\mathbf{x});\mathbf{q}_1,\mathbf{q}_2) \right] \phi(\mathbf{q}_1)\phi(\mathbf{q}_2) e^{i(\mathbf{q}_1+\mathbf{q}_2)\mathbf{x}} \\ & + V^{-2} \sum_{\mathbf{q}_1,\mathbf{q}_2,\mathbf{q}_3,\mathbf{q}_4} \left[\theta_k^{(3)}(\rho(\mathbf{x});\mathbf{q}_1,\mathbf{q}_2,\mathbf{q}_3) + \theta_k^{(4)}(\rho(\mathbf{x});\mathbf{q}_1,\mathbf{q}_2,\mathbf{q}_3,\mathbf{q}_4) \right] \\ & \times \phi(\mathbf{q}_1)\phi(\mathbf{q}_2)\phi(\mathbf{q}_3)\phi(\mathbf{q}_4) e^{i(\mathbf{q}_1+\mathbf{q}_2+\mathbf{q}_3+\mathbf{q}_4)\mathbf{x}} + \cdots \Bigg) d\mathbf{x}\,, \end{aligned} \tag{28}$$

where $\rho(\mathbf{x}) = \phi^2(\mathbf{x})/2$, and the functions $\theta_k^{(\ell)}$ have the property: $\theta_k^{(\ell)}(\rho(\mathbf{x});\mathbf{q}_1,\mathbf{q}_2,\ldots,\mathbf{q}_\ell) = 0$, if $\mathbf{q}_j = 0$ holds for any of $j \in [1,\ell]$. Based on this general form, a new truncation scheme has been developed in [10], where the terms with $\ell \leqslant m$ are included at the mth order of truncation.

The case $m=1$ has been considered in detail [10], denoting $\theta_k^{(1)}(\rho;\mathbf{q}) = \theta_k(\rho;\mathbf{q})$ and deriving the RG flow equations for $U_k(\rho)$ and $\theta_k(\rho;\mathbf{q})$. Further on, a new variable

$$\Psi_k(\rho;\mathbf{q}) = \theta_k(\rho;\mathbf{q}) + 2\,\rho\theta_k'(\rho;\mathbf{q}) \tag{29}$$

has been introduced for a simplification, where $\theta_k'(\rho;\mathbf{q}) = \frac{\partial}{\partial\rho}\theta_k(\rho;\mathbf{q})$.

Moreover, the resulting RG flow equations in [10] have been written in a scaled (dimensionless) form, using the transformations

$$U_k(\rho) = k^d u_k(\tilde{\rho})\,, \qquad \text{where} \quad \tilde{\rho} = Z_k k^{2-d}\rho\,, \tag{30}$$

$$R_k(q) = Z_k q^2 r(y)\,, \qquad \text{where} \quad y = q^2/k^2\,, \tag{31}$$

$$\Psi_k(\rho;\mathbf{q}) = \frac{1}{2} Z_k q^2 f_k(\tilde{\rho};y)\,, \tag{32}$$

where Z_k is defined as

$$Z_k = \lim_{q\to 0}\left(\frac{2}{q^2}\Psi_k(0;\mathbf{q})\right)\,. \tag{33}$$

In addition, the running exponent $\eta(k)$ is defined by the equation

$$\frac{d}{dt}\ln Z_k = -\eta(k)\,, \tag{34}$$

where $t = \ln(k/\Lambda)$. The dimensionless cut-off function, corresponding to (4), is

$$r(y) = \alpha/\left(e^y - 1\right)\,. \tag{35}$$

The above transformations have led to the following RG flow equations [10]:

$$\frac{\partial u_k(\tilde{\rho})}{\partial t} = -d\,u_k(\tilde{\rho}) + (d-2+\eta(k))\tilde{\rho}\,u_k'(\tilde{\rho}) - \frac{K_d}{4}\int\limits_0^{\Lambda^2/k^2}\frac{y^{\frac{d}{2}-1}\zeta_k(y)dy}{\mathcal{P}_k(\tilde{\rho},y)}\,, \tag{36}$$

$$\begin{aligned}\frac{\partial f_k(\tilde{\rho};y)}{\partial t} &= \eta(k) f_k(\tilde{\rho};y) + \tilde{\rho}(d-2+\eta(k)) f_k'(\tilde{\rho};y) + 2y\frac{\partial f_k(\tilde{\rho};y)}{\partial y} \\ &+ \frac{K_d}{4}\left(f_k'(\tilde{\rho};y) + 2\,\tilde{\rho} f_k''(\tilde{\rho};y)\right)\int\limits_0^{\Lambda^2/k^2}\frac{y_1^{\frac{d}{2}-1}\zeta_k(y_1)dy_1}{\mathcal{P}_k^2(\tilde{\rho},y_1)} \\ &- y^{-1}\left[\hat{C}_k(\tilde{\rho},y) - \hat{C}_k(\tilde{\rho},0)\right]\,,\end{aligned} \tag{37}$$

where

$$\zeta_k(y) = 2y^2\,r'(y) + \eta(k)\,y r(y)\,, \tag{38}$$

$$w_k(\tilde{\rho}) = u_k'(\tilde{\rho}) + 2\,\tilde{\rho}\,u_k''(\tilde{\rho})\,, \tag{39}$$

$$\mathcal{P}_k(\tilde{\rho},y) = w_k(\tilde{\rho}) + y[f_k(\tilde{\rho};y) + r(y)] \tag{40}$$

and

$$\begin{aligned}\hat{C}_k(\tilde{\rho},y) = \tilde{\rho}\tilde{K}_d \int\limits_0^{\Lambda^2/k^2}\int\limits_0^{\pi}\zeta_k(y_1)\,\Theta\left(\frac{\Lambda^2}{k^2} - Y\right) y_1^{\frac{d}{2}-1}(\sin\theta)^{d-2} \\ \times\frac{\left(w_k'(\tilde{\rho}) + \frac{1}{2}\left[y f_k'(\tilde{\rho};y) + y_1 f_k'(\tilde{\rho};y_1) + Y f_k'(\tilde{\rho};Y)\right]\right)^2}{\mathcal{P}_k(\tilde{\rho},Y)\,\mathcal{P}_k^2(\tilde{\rho},y_1)}\,dy_1 d\theta\,,\end{aligned} \tag{41}$$

where $Y = y + y_1 + 2\sqrt{yy_1}\cos\theta$. Here primes denote derivatives with respect to $\tilde{\rho}$, except for $r'(y) = dr/dy$, and Θ is the Heaviside theta function. In addition, $K_d = S(d)/(2\,\pi)^d$ and

$\tilde{K}_d = S(d-1)/(2\,\pi)^d$, where $S(d)$ is the surface of unit sphere in d dimensions. The equation for $\eta(k)$ reads

$$\eta(k) = -\frac{K_d}{4} f_k'(0;0) \int\limits_0^{\Lambda^2/k^2} \frac{y^{\frac{d}{2}-1}\zeta_k(y)dy}{\mathcal{P}_k^2(0,y)}\,. \tag{42}$$

Note that the integral in this expression depends on $\eta(k)$ via $\zeta_k(y)$.

In [10], these RG flow equations have been solved, approximating the dimensionless potential $u_k(\tilde{\rho})$ by a second-order polynomial of $\tilde{\rho}$ and $f_k(\tilde{\rho};y)$ by a linear function of $\tilde{\rho}$. This has been done just to show that a reasonable solution exists. Refined approximations are considered in this work.

Appendix B. Calculation of the coefficients in the RG flow equations

The coefficients in (21)–(23) are found by the following algorithm. First we calculate recursively the expansion coefficients of $(1-s)^\mu$, i.e.

$$a_0(\mu) = 1\,, \quad a_j(\mu) = \frac{j-1-\mu}{j}\,a_{j-1}(\mu)\,, \quad j = 1,2,\ldots,\tilde{n}\,, \tag{43}$$

where $\tilde{n} = \max\{n,n'\}$. Then we compute the expansion coefficients $\tilde{u}_{i,k}$ of $\bar{u}_k(s)$, i.e.

$$\begin{aligned} &\tilde{u}_{0,k} = 0\,, \quad \tilde{u}_{i,k} = \sum_{j=0}^{i-1} a_j(-\mu)u_{i-j,k}\,, \quad i = 1,2,\ldots,\tilde{n}+1\,; \\ &u_{m,k} = 0 \text{ for } m > n \end{aligned} \tag{44}$$

and, subsequently, those of $s(1-s)\bar{u}_k'(s)$, $(1-4s)\bar{u}_k'(s) + 2s(1-s)\bar{u}_k''(s)$, $\bar{w}_k(s)$ and $\bar{\mathcal{P}}_k(s,y)$:

$$c_{i,k} = i\tilde{u}_{i,k} - (i-1)\tilde{u}_{i-1,k}\,, \quad i = 1,2,\ldots,n\,, \tag{45}$$

$$e_{i,k} = (i+1)\Big((2i+1)\tilde{u}_{i+1,k} - 2i\,\tilde{u}_{i,k}\Big)\,, \quad i = 0,1,\ldots,\tilde{n}\,, \tag{46}$$

$$w_{i,k} = (e_{i,k} - 2e_{i-1,k} + e_{i-2,k})/\tilde{\rho}_0\,, \quad i = 0,1,\ldots,\tilde{n}; \quad e_{-1,k} = e_{-2,k} = 0\,, \tag{47}$$

$$\mathcal{P}_{i,k}(y) = w_{i,k} + y\,[f_{i,k}(y) + \delta_{i,0}\,r(y)]\,, \quad i = 0,1,\ldots,\tilde{n}\,. \tag{48}$$

Now we are ready to calculate $\mathcal{L}_{i,k}$ in (21), i.e.

$$\mathcal{L}_{i,k} = \sum_{j=0}^{i-1} a_j(\mu)\tilde{\mathcal{L}}_{i-j,k}\,, \quad i = 1,2,\ldots,n\,, \tag{49}$$

where $\tilde{\mathcal{L}}_{i,k}$ are the expansion coefficients of $(1-s)^{-\mu}\mathcal{L}_k(s)$. Using (13), we obtain

$$\tilde{\mathcal{L}}_{i,k} = \sum_{\substack{j_1,j_2,\ldots,j_i \\ \sum_{\ell=1}^i \ell j_\ell = i}} \frac{(-1)^m m!}{\prod_{\ell=1}^i j_\ell!}\,L_k(m,j_1,j_2,\ldots,j_i)\,, \quad i = 1,2,\ldots,n\,, \tag{50}$$

where $j_\ell \geqslant 0$ are integer numbers, $m = \sum_{\ell=1}^i j_\ell$ and

$$L_k(m,j_1,j_2,\ldots,j_i) = \frac{K_d}{4}\int\limits_0^\infty \frac{y^{\frac{d}{2}-1}\zeta_k(y)\prod_{\ell=1}^i \mathcal{P}_{\ell,k}^{j_\ell}(y)}{[\mathcal{P}_{0,k}(y)]^{m+1}}\,\tilde{\Theta}\left(\frac{\Lambda^2}{k^2} - y\right)dy\,. \tag{51}$$

The sharp cut-off in (13) is obtained when $\tilde{\Theta}(x)$ is set equal to the Heaviside theta function. However, we have used a smooth cut-off function

$$\tilde{\Theta}(x) = \frac{1}{2}\Big(\tanh(x)+1\Big) \tag{52}$$

instead.

By (43)–(52) we can completely calculate the right hand side of (21) at the given $u_{i,k}, f_{i,k}(y)$ and $\eta(k)$. The coefficients in (22) and (23) are calculated by the same approach, as summarized below:

$$\varepsilon_{i,k}(y) = (i+1)\Big((2i+1)f_{i+1,k}(y) - 2i f_{i,k}(y)\Big), \quad i=0,1,\ldots,n', \tag{53}$$

$$\omega_{i,k}(y) = (\varepsilon_{i,k}(y) - 2\,\varepsilon_{i-1,k}(y) + \varepsilon_{i-2,k}(y))/\tilde{\rho}_0, \qquad i=0,1,\ldots,n', \tag{54}$$

where $f_{n'+1,k}(y)=0$, and $\varepsilon_{j,k}(y)=0$ for $j<0$;

$$Q_{i,k}(y) = \sum_{\ell=0}^{i} \mathcal{P}_{\ell,k}(y)\mathcal{P}_{i-\ell,k}(y), \quad i=0,1,\ldots,n', \tag{55}$$

$$\mathcal{M}_{0,k} = \frac{K_d}{4}\int_0^\infty \frac{y^{\frac{d}{2}-1}\zeta_k(y)}{Q_{0,k}(y)}\,\tilde{\Theta}\left(\frac{\Lambda^2}{k^2}-y\right)dy, \tag{56}$$

$$\mathcal{M}_{i,k} = \sum_{\substack{j_1,j_2,\ldots,j_i \\ \sum_{\ell=1}^{i}\ell j_\ell = i}} \frac{(-1)^m m!}{\prod_{\ell=1}^{i} j_\ell!}\,M_k(m,j_1,j_2,\ldots,j_i), \quad i=1,2,\ldots,n', \tag{57}$$

where $j_\ell \geqslant 0$ are integer numbers, $m=\sum_{\ell=1}^{i} j_\ell$ and

$$M_k(m,j_1,j_2,\ldots,j_i) = \frac{K_d}{4}\int_0^\infty \frac{y^{\frac{d}{2}-1}\zeta_k(y)\prod_{\ell=1}^{i} Q_{\ell,k}^{j_\ell}(y)}{[Q_{0,k}(y)]^{m+1}}\,\tilde{\Theta}\left(\frac{\Lambda^2}{k^2}-y\right)dy; \tag{58}$$

$$\grave{Q}_{i,k}(y_1,Y) = \sum_{\ell=0}^{i} \mathcal{P}_{\ell,k}(Y)Q_{i-\ell,k}(y_1), \quad i=0,1,\ldots,n'-1, \tag{59}$$

$$A_{0,k}(y_1,Y) = \frac{1}{\mathcal{P}_{0,k}(Y)\,\mathcal{P}_{0,k}^2(y_1)}, \tag{60}$$

$$A_{i,k}(y_1,Y) = \sum_{\substack{j_1,j_2,\ldots,j_i \\ \sum_{\ell=1}^{i}\ell j_\ell = i}} \frac{(-1)^m m!\prod_{\ell=1}^{i}[\grave{Q}_{\ell,k}(y_1,Y)]^{j_\ell}}{[\grave{Q}_{0,k}(y_1,Y)]^{m+1}\prod_{\ell=1}^{i} j_\ell!}, \quad i=1,2,\ldots,n'-1, \tag{61}$$

where $j_\ell \geqslant 0$ are integers, $m=\sum_{\ell=1}^{i} j_\ell$ and $Y = y + y_1 + 2\sqrt{yy_1}\cos\theta$;

$$W_{i,k}(y,y_1,Y) = (i+1)\left[w_{i+1,k} + \frac{1}{2}\Big(y f_{i+1,k}(y) + y_1 f_{i+1,k}(y_1) + Y f_{i+1,k}(Y)\Big)\right], \tag{62}$$

$$B_{i,k}(y,y_1,Y) = \sum_{\ell=0}^{i} W_{\ell,k}(y,y_1,Y)\,W_{i-\ell,k}(y,y_1,Y), \tag{63}$$

$$\grave{W}_{i,k}(y,y_1,Y)=\sum_{\ell=0}^{i}B_{\ell,k}(y,y_1,Y)A_{i-\ell,k}(y_1,Y)\,, \tag{64}$$

$$I_{i,k}(y)=\tilde{K}_d\int_0^{\infty}\int_0^{\pi}y_1^{\frac{d}{2}-1}\zeta_k(y_1)(\sin\theta)^{d-2}\,\grave{W}_{i,k}(y,y_1,Y) \times\tilde{\Theta}\left(\frac{\Lambda^2}{k^2}-Y\right)\tilde{\Theta}\left(\frac{\Lambda^2}{k^2}-y_1\right)dy_1d\theta\,, \tag{65}$$

where $i=0,1,\ldots,n'-1$ in equations (62)–(65);

$$C_{i,k}(y)=[I_{i-1,k}(y)-3I_{i-2,k}(y)+3I_{i-3,k}(y)-I_{i-4,k}(y)]/\tilde{\rho}_0\,, \quad i=1,2,\ldots,n'\,, \tag{66}$$

where $I_{j,k}(y)=0$ for $j<0$;

$$\mathcal{F}_{i,k}(y)=y^{-1}[C_{i,k}(y)-C_{i,k}(0)]\,,\quad i=1,2,\ldots,n'\,. \tag{67}$$

By this, all coefficients on the right-hand side of (21)–(23) are calculated.

Appendix C. The purely numerical solution of the LPA equation

We consider the LPA equation, which can be written as

$$\frac{\partial u_k(\tilde{\rho})}{\partial t}=-d\,u_k(\tilde{\rho})+(d-2)\,\tilde{\rho}\,u_k'(\tilde{\rho})+F_k(\tilde{\rho})\,, \tag{68}$$

where

$$F_k(\tilde{\rho})=-\frac{K_d}{2}\int_0^{\Lambda^2/k^2}\frac{y^{\frac{d}{2}-1}\,r'(y)\,dy}{u_k'(\tilde{\rho})+2\,\tilde{\rho}\,u_k''(\tilde{\rho})+y[1+r(y)]}\,. \tag{69}$$

We have assumed as a self-consistent boundary condition that $F_k(\tilde{\rho})$ together with all its derivatives tend to zero at $\tilde{\rho}\to\infty$. According to the vanishing derivative, we have set $F_k(\tilde{\rho})\equiv F_k(\tilde{\rho}')$ for $\tilde{\rho}>\tilde{\rho}'$. Here $\tilde{\rho}'$ is a large enough maximal $\tilde{\rho}$ value for which $F_k(\tilde{\rho})$ can be calculated, using the specific representation of $F_k(\tilde{\rho})$ by finite differences on the given grid. A simpler condition would be $F_k(\tilde{\rho})\equiv 0$ for $\tilde{\rho}>\tilde{\rho}'$, but the former one is a better approximation for $\tilde{\rho}\gtrsim\tilde{\rho}'$.

We have used the grid of $\tilde{\rho}$ values with the origin at $\tilde{\rho}_0=0$, the next values being $\tilde{\rho}_1$, $\tilde{\rho}_2$, $\tilde{\rho}_3$, etc with $\tilde{\rho}_{i+1}-\tilde{\rho}_i=(\tilde{\rho}_i-\tilde{\rho}_{i-1})(1+\varepsilon)$, where ε is a small enough positive constant. The construction of the grid is continued until a certain maximal value $\tilde{\rho}_{\max}$ is exceeded. We have used $\tilde{\rho}_{\max}=2$ as a standard value, noting that the increase in $\tilde{\rho}_{\max}$ to $\tilde{\rho}_{\max}=5$ has not lead to detectable differences in the results.

The derivative in (68) is expressed as $u_k'(\tilde{\rho}_i)=(u_k(\tilde{\rho}_i)-u_k(\tilde{\rho}_{i-1}))/h_i$, where $h_i=\tilde{\rho}_i-\tilde{\rho}_{i-1}$ is the ith step size and $i\geqslant 1$. Here we set $\tilde{\rho}\,u_k'(\tilde{\rho})=0$ at $\tilde{\rho}=0$. We have used a different representation of this derivative in the calculation of the integral (69), i.e. $u_k'(\tilde{\rho}_i)=(u_k(\tilde{\rho}_{i+1})-u_k(\tilde{\rho}_i))/h_{i+1}$, where $i\geqslant 0$. Formally, these representations are consistent for $i\geqslant 1$ at $h_i\to 0$. The second derivative in (69) is expressed as

$$u_k''(\tilde{\rho}_i)=\frac{2}{\tilde{\rho}_{i+1}-\tilde{\rho}_{i-1}}\left(\frac{u_k(\tilde{\rho}_{i+1})-u_k(\tilde{\rho}_i)}{\tilde{\rho}_{i+1}-\tilde{\rho}_i}-\frac{u_k(\tilde{\rho}_i)-u_k(\tilde{\rho}_{i-1})}{\tilde{\rho}_i-\tilde{\rho}_{i-1}}\right),\quad i\geqslant 1. \tag{70}$$

In the case of a constant step size h, equation (70) reduces to the known standard expression $u_k''(\tilde{\rho}_i) = (u_k(\tilde{\rho}_{i+1}) - 2\,u_k(\tilde{\rho}_i) + u_k(\tilde{\rho}_{i-1}))/h^2$. The used here representation of the derivatives by finite differences is such that it ensures the numerical stability at small enough magnitude of the integration step Δt, noting that t decreases. It is expected from a simple argument, according to which a perturbation in a form of a small deviation of the ith point from a smooth curve tends to be smoothen out in the following integration steps if $\Delta t \propto h_i^2$ is small enough in magnitude and negative. Note, e.g. that the usage of $u_k'(\tilde{\rho}_i) = (u_k(\tilde{\rho}_{i+1}) - u_k(\tilde{\rho}_i))/h_{i+1}$ for the explicit derivative term in (68) leads to a numerical instability, according to such an analysis. The conclusions of this stability analysis have been fully confirmed by numerical tests.

We have used a second-order Runge-Kutta method (i.e. for $dx/dt = f(t,x)$, $x_{n+1} = x_n + \frac{1}{2}\Delta t\,(k_1 + k_2)$, where $k_1 = f(t_n, x_n)$, $k_2 = f(t_{n+1}, x_n + \Delta t\, k_1)$) for the integration of the RG flow equation (68). As we have found out, the results of our simple difference scheme remarkably depend on the grid step sizes. Smaller values of $\tilde{\rho}_1$ and ε generate a finer grid. To obtain accurate results, an extrapolation to $\tilde{\rho}_1 \to 0$ and $\varepsilon \to 0$ has been performed, using the grid parameters $\varepsilon = 0.025$, 0.0125 and 0.006 25 with $\tilde{\rho}_1 = 0.1\,\varepsilon$. The integration step has been chosen $\Delta t = -2\,\varepsilon^2$ to ensure the numerical stability.

A grid of y values: $y_0 = 0, y_1, y_2$, etc has been used for calculation of the integral (69), where each next step size increases by the factor $1 + \varepsilon'$ as compared to the previous one, but not exceeding certain maximal value $(\Delta y)_{\max}$. As a standard, we have set $(\Delta y)_1 = 0.001$, $(\Delta y)_{\max} = 0.4$ and $\varepsilon' = 0.2$. The integration region has been limited by the maximal y value $y_{\max} = 25$. We have applied the Simpson rule for the evaluation of the contribution of each sub-interval $y \in [y_i, y_{i+1}]$, which requires also an evaluation at $y = (y_i + y_{i+1})/2$. The set of standard step sizes considered here for the y grid ensures a sufficient numerical accuracy, as it has been verified by testing different step sizes.

Appendix D. Iterative finding of the fixed point and extraction of the critical exponents

Integrating the RG flow equations, we always start with the initial condition $u_{k_0}(\tilde{\rho}) = b_1\ \tilde{\rho} + b_2\ \tilde{\rho}^2 + b_3\ \tilde{\rho}^3$ in the purely numerical LPA case and with $\hat{u}_{k_0}(s) = u_{1,k_0}s + u_{2,k_0}s^2 + u_{3,k_0}s^3$, $\bar{f}_{k_0}(s;y) = 1$ in the case of the functional truncations, the initial k value being equal to $k_0 = \Lambda = 1$.

The critical value of u_{1,k_0} has been found to reach the fixed point by the following iterative algorithm. Starting with some approximation for u_{1,k_0}, the integration of the RG flow equations is performed until either a certain (negative) final value t_{min} of t is reached or $|\,\partial u_{1,k}/\partial t\,|$ becomes too large. Then the value of u_{1,k_0} is corrected, taking into account how $k^{1/\nu}\partial u_{1,k}/\partial t$ at the end point of the integration changes with u_{1,k_0}, with an aim to satisfy the condition $k^{1/\nu}\partial u_{1,k}/\partial t = 0$. Here ν is the critical exponent. The same iterative algorithm with b_1 instead of u_{1,k_0} and with $a_{1,k} = (u_k(\tilde{\rho}_1) - u_k(0))/\tilde{\rho}_1$ (where $\tilde{\rho}_1$ is the first non-zero grid point) instead of $u_{1,k}$ has been applied in the purely numerical case. We have used $u_{2,k_0} = b_2 = 0.2$ and $u_{3,k_0} = b_3 = 1$. Besides, we have set $t_{min} = -20$ for the purely numerical solution and $t_{min} = -17$ in other cases. The precision in ν only slightly influences the rate of the convergence. We have used an approximate ν value, i.e. 0.65 in the LPA case and $\nu = 0.63$ in the non-LPA case.

The critical exponent $y_T = 1/\nu$ describes the $\propto k^{-y_T}$ small deviations from the critical surface at small k. We have determined it from the $\propto k^{-y_T}$ scaling of $\tilde{a}_{1,k} - a_{1,k}$ (for the purely numerical LPA solution) or $\tilde{u}_{1,k} - u_{1,k}$ (for the functional truncations), where the quantities marked by tilde are calculated by slightly shifting b_1 or u_{1,k_0}, respectively, from their

critical values. The shifts $\Delta b_1 = 10^{-13}$ and $\Delta u_{1,k_0} = 10^{-12}$ have been applied. The running exponent $y_T(t)$ has been determined by using the ansatz $\tilde{a}_{1,k} - a_{1,k} = const \cdot k^{-y_T}$ or $\tilde{u}_{1,k} - u_{1,k} = const \cdot k^{-y_T}$ for two values of k, corresponding to $t \pm \Delta t$ with $\Delta t \approx 0.7$. We have $y_T(k) = F_y(k)$, where $F_y(k) = \ln\left[(\tilde{v}_{k_2} - v_{k_2})/(\tilde{v}_{k_1} - v_{k_1})\right]/[2\ \Delta t]$ and $k_{1,2} = k\exp(\pm\Delta t)$ with $v_k = a_{1,k}$, $\tilde{v}_k = \tilde{a}_{1,k}$ or $v_k = u_{1,k}$, $\tilde{v}_k = \tilde{u}_{1,k}$ in these two cases.

For the integration of the RG flow, we need to know the critical exponent η, entering $\mu = d/(d-2+\eta)$, which we do not know beforehand. We have used the following trick here. First, a trial calculation (iteration) with $\mu = d/(d-2+\eta(k))$ is performed, where $\eta(k)$ is the running exponent. Since $\eta(k) \to \eta$, it gives the correct fixed point and η, although the RG flow to it is not fully correct because the RG flow equations are derived for a constant μ. After this, the real calculation with the found constant value of η is performed. In fact, it turned out that the precise value of η in $\mu = d/(d-2+\eta)$ has a minor importance in three dimensions. The results practically did not change when $\mu = d/(d-2)$ was used instead of $\mu = d/(d-2+\eta)$ in some test calculations. However, it is important for the critical exponent ω, at least, that μ is kept constant.

The critical exponent ω, known also as the correction-to-scaling exponent, describes the $\propto k^{\omega}$ distance from the fixed point at $k \to 0$, considering the RG flow on the critical surface, i.e. at the critical values of b_1 or u_{1,k_0} in our schemes. Correspondingly, the running exponent $\omega(t)$ has been determined by using the ansatz $a_{1,k} = a_1^* + const \cdot k^{\omega}$ or $u_{1,k} = u_1^* + const \cdot k^{\omega}$ for three values of k, corresponding to t and $t \pm \Delta t$ with $\Delta t \approx 0.7$. We have $\omega(k) = F_\omega(k)$, where $F_\omega(k) = \ln\left[(v_{k_1} - v_k)/(v_k - v_{k_2})\right]/\Delta t$ and $k_{1,2} = k\exp(\pm\Delta t)$ with $v_k = a_{1,k}$ or $v_k = u_{1,k}$ in these two cases.

Appendix E. Integration of the RG flow equations

For the integration of the RG flow equations (21)–(23), a certain grid of y values is used, which is similar to the grid of $\tilde{\rho}$ values considered in appendix C. Namely, the origin is at $y = 0$, and the following grid points $y_1, y_2, \ldots, y_M$ are such that each next step size is by a factor $1+\varepsilon$ larger than the previous one. The construction of the grid is continued until $B/k_{\min}^2$ is exceeded, where B is a large constant and $k_{\min} = \exp(t_{\min})$ is the smallest k value reached. This choice of $y_M \geqslant B/k_{\min}^2$ means that the wave vectors with the magnitude $q \leqslant \sqrt{B}$ are included. We have typically used $B = 10^5$, $t_{\min} = -17$, $y_1 = 0.01$ and $\varepsilon = 0.2$. This grid-construction allows to reach small enough step sizes for small y values, ensures that the relative y variation between the neighboring grid points is about ε for larger y values and, simultaneously, allows to reach very large y values, using not too many grid points. The RG flow equations require also the integration over the internal y variable, for which purpose the grid of y values is used, already introduced in appendix C. In addition, the integration over the angle θ is performed by the Simpson method, using the step size $\Delta\theta = \pi/10$. The considered above step sizes refer to the so called standard grid. All step sizes are twice as large for the rough grid, used in some calculations—see section 5.2.

Equation (22) contains the derivative $\partial f_{i,k}(y)/\partial y$, which is expressed by finite differences as

$$\left.\frac{\partial f_{i,k}(y)}{\partial y}\right|_{y=y_i} = \frac{f_{i,k}(y_i) - f_{i,k}(y_{i-1})}{y_i - y_{i-1}}, \quad i = 1,2,\ldots,M, \tag{71}$$

noting that $y\,\partial f_{i,k}(y)/\partial y = 0$ at $y = 0$. It ensures the numerical stability at a small enough magnitude of the integration step $\Delta t < 0$, as it follows from numerical tests, as well as from simple stability arguments introduced in appendix C. The integration has been performed

by the fourth-order (or the second-order at $n' = 0$) Runge-Kutta method with the step size $\Delta t = -0.005$ for $n \leqslant 10$ and $\Delta t = -0.0025$ for $n \geqslant 11$.

The integrals in appendix B have been calculated by the Simpson method, using the Newton's second-order interpolation polynomial for the evaluation of $f_{i,k}(y)$ between the grid points. We need also to know the values of $f_{i,k}(y)$ for $y > y_M$ to calculate these integrals. The condition $y_M \geqslant B/k_{\min}^2$ with large B ensures that $f_{0,k}(y) \approx const$ holds for $y > y_M$, as well as that $f_{i,k}(y)$ with $i \geqslant 1$ tends to zero as $\sim 1/y$ for $y > y_M$. Thus, we have set $f_{0,k}(y) = f_{0,k}(y_M)$ for $y > y_M$ and $f_{i,k}(y) = f_{i,k}(y_M)\, y_M/y$ for $i \geqslant 1$, $y > y_M$.

ORCID iD

J Kaupužs https://orcid.org/0000-0001-6047-3043

References

[1] Amit D J 1984 *Field Theory, the Renormalization Group and Critical Phenomena* (Singapore: World Scientific)
[2] Sornette D 2000 *Critical Phenomena in Natural Sciences* (Berlin: Springer)
[3] Ma S-K 1976 *Modern Theory of Critical Phenomena* (New York: W.A. Benjamin, Inc.)
[4] Zinn–Justin J 1996 *Quantum Field Theory and Critical Phenomena* (Oxford: Clarendon)
[5] Kleinert H and Schulte–Frohlinde V 2001 *Critical Properties of* ϕ^4 *Theories* (Singapore: World Scientific)
[6] Wetterich C 1993 Phys *Lett.* B **301** 90
[7] Polchinski J 1984 *Nucl. Phys.* B **231** 269
[8] Bagnuls C and Bervillier C 2001 *Phys. Rep.* **348** 91
[9] Berges J, Tetradis N and Wetterich C 2002 *Phys. Rep.* **363** 223
[10] Kaupužs J and Melnik R V N 2020 *J. Phys. A: Math. Theor.* **53** 415002
[11] Balog I, Chate H, Delamotte B, Marohnic M and Wschebor N 2019 *Phys. Rev. Lett.* **123** 240604
[12] Papenbrock T and Wetterich C 1995 *Z. Phys.* C **65** 519–35
[13] Litim D 2001 *Phys. Rev.* D **64** 105007
[14] Canet L, Delamotte B, Mouhanna D and Vidal J 2003 *Phys. Rev.* D **67** 065004
[15] Canet L, Delamotte B, Mouhanna D and Vidal J 2003 *Phys. Rev.* B **68** 064421
[16] Litim D F 2002 arXiv:hep-th/0203006
[17] Bender C M and Sarkar S 2018 *J. Phys. A: Math. Theor.* **51** 225202
[18] Benitez F, Blaizot J-P, Chate H, Delamotte B, Mendez-Galain R and Wschebor N 2012 *Phys. Rev.* E **85** 026707
[19] De Polsi G, Balog I, Tissier M and Wschebor N 2020 *Phys. Rev. E.* **101** 042113
[20] Berges J, Jungnickel D-U and Wetterich C 1999 *Phys. Rev.* D **59** 034010
[21] Schütz F and Kopietz P 2006 *J. Phys. A: Math. Gen.* **39** 8205
[22] Benedetty D, Groh K, Machado P F and Saueressig F 2011 *J. High Energy Phys.* JHEP06(2011)079
[23] Demmel M, Saueressig F and Zanusso O 2014 *J. High Energy Phys.* JHEP06(2014)026
[24] Wetterich C and Yamada M 2019 *Phys. Rev.* D **100** 066017
[25] Platania A B 2018 *Asymptotically Safe Gravity: From Spacetime Foliation to Cosmology* (Cham: Springer Theses-Recognizing Outstanding PhD Research) pp 29–46
[26] Wetterich C 2017 *Phys. Rev.* D **95** 123525
[27] Eichhorn A 2019 *Front. Astron. Space Sci.* **5** 47
[28] Alwis S P 2018 *J. High Energy Phys.* JHEP03(2018)118
[29] Litim D F and Trott M J 2018 *Phys. Rev.* D **98** 125006
[30] Bond A D and Litim D F 2019 *Phys. Rev. Lett.* **122** 211601
[31] Falls K G, Litim D F and Schroder J 2019 *Phys. Rev.* D **99** 126015
[32] Lahoche V and Samary D O 2019 *Universe* **5** 86
[33] Poland D and Simmons-Duffin D 2016 *Nat. Phys.* **12** 535
[34] Kaupužs J and Melnik R V N 2022 arXiv:2206.04393 [cond-mat.stat-mech]